Evolutions of helical edge states in disordered HgTe/CdTe quantum wells

Liang Chen,[1,2] Qin Liu,[1] * Xulin Lin[1,2], Xiaogang Zhang[1,2], Xunya Jiang[1]

[1] *State Key Laboratory of Functional Materials for Informatics,*
Shanghai Institute of Microsystem and Information Technology, CAS, Shanghai 200050, China and
[2] *Graduate School of Chinese Academy of Sciences, Beijing 100049, People's Republic of China*
(Dated: June 22, 2011)

We study the evolutions of the nonmagnetic disorder-induced edge states with the disorder strength in the HgTe/CdTe quantum wells. From the supercell band structures and wave-functions, it is clearly shown that the conducting helical edge states, which are responsible for the reported quantized conductance plateau, appear above a critical disorder strength after a gap-closing phase transition. These edge states are then found to decline with the increase of disorder strength in a stepwise pattern due to the finite-width effect, where the opposite edges couple with each other through the localized states in the bulk. This is in sharp contrast with the localization of the edge states themselves if magnetic disorders are doped which breaks the time-reversal symmetry. The size-independent boundary of the topological phase is obtained by scaling analysis, and an Anderson transition to an Anderson insulator at even stronger disorder is identified, in-between of which, a metallic phase is found to separate the two topologically distinct phases.

PACS numbers: 73.43.Nq, 72.25.-b, 71.30.th, 72.15.Rn

I. INTRODUCTION

Disorder effect is one of the most important problems in the subject of topological insulators (TI)[1]. Recently a nonmagnetic *disorder-induced* topological insulator state, named as the topological Anderson insulator (TAI), is found by computer simulations in both two-[2] and three-dimensional (3D)[3] systems, and is further confirmed through independent simulations by studying the local currents[4]. This state is numerically characterized by precisely quantized conductance e^2/h[2–4], and is theoretically understood as generated by the negative renormalized topological mass[3,5] within the self-consistent Born approximation (SCBA). Phase diagrams for these systems on the energy-disorder plane at fixed mass parameter are obtained[2,3,5], where the TAI phase appears as an island between the so-called weak- and strong-disorder boundaries[5]. The locations of these boundaries depend generally on the size of the system under simulation. Topological invariants in disordered systems are also discussed[6,7]. In particular, it is argued that the 2D TAI phase is not a distinct one, but is instead part of the quantum spin Hall phase[6] with nontrivial spin-Chern number[8] in the presence of disorder if the phase diagram is extended to the mass axis.

Despite all these achievements on understanding the surprising disorder-induced topological phase, there still exist some questions. First, it has been experimentally proved that the quantized conductance, $2e^2/h$, in clean 2D HgTe/CdTe quantum wells (QWs)[9] measured in transport studies[10] is the direct consequence of gapless conducting edge states. However in the disorder-induced TI, the existence of such edge states in energy-
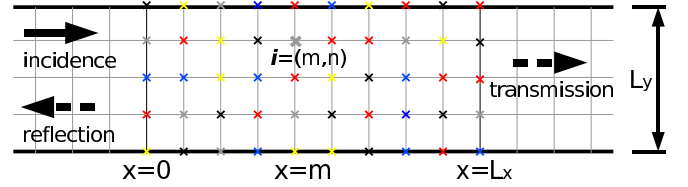

FIG. 1: (color online). Schematic illustration of the two-terminal device. The central stripe is made of HgTe/CdTe QWs with length L_x and width L_y where nonmagnetic disorders exist. Two semi-infinite clean leads made of the same materials are fabricated which are heavily doped to access the $|E_f| < M$ region[5].

momentum space, their evolution with disorder strength, as well as how the evolution picture corresponds to the wave-function behaviors in real space have not been well investigated yet. Second, when deviating the TAI region, how these edge states terminate with the increase of the disorder strength and what is their difference from that of the usual bulk states are also not resolved so far. Finally, as mentioned in Ref.[5], the weak-disorder boundary is not an Anderson transition at all as the name TAI might suggest, in the sense that it is more of a band-effect rather than the result of a mobility edge. Therefore the Anderson transition boundary, which is expected to be the true size-independent phase boundary of TAI in strong-disorder region, is still absent for now.

Motivated by these issues, in this paper, we study the disorder-induced conducting edge states and the phase boundaries of the TAI in the effective model of disordered HgTe/CdTe QWs. First, the existence of gapless helical edge states is demonstrated in energy-momentum space through a gap-closing phase transition when above a critical disorder strength. This result appraises the topological aspect of the TAI in a straightforward way, and is the fundamental reason of the observed quan-

*E-mail: liuqin@mail.sim.ac.cn

tized anomalous conductance plateaus in previous transport studies[2–5]. Second, the evolution of such disorder-induced edge states with disorder strength is also studied, where how the edge states decay in strong-disorder region is focused on in particular. It is shown that for a finite-width system, unlike the usual exponential decay in quasi-1D disordered systems[11], the nontrivial edge states decay in a *stepwise* pattern due to the competition between the sample width L_y and the localization length $\xi(W)$. Finally, we locate the true Anderson transition boundaries by scaling analysis for an infinite system. These boundaries indicate that the system undergoes a multiple transitions, first from metal to topological insulator, then to metal again, and finally localizes as an Anderson insulator. It is interesting to compare with the work by Yamakage[12] *et al* that our result shows that a spin-s_z nonconservation term is not necessarily needed to have a metallic region which separates two topologically distinct insulating phases.

The rest of this paper is organized as follows. In section II, we introduce our simulating model and methods. In section III, we present our numerical results and theoretical analyses. Finally, this work is concluded in section IV.

II. MODEL AND METHOD

Our starting point is the 2D effective Hamiltonian of HgTe/CdTe QWs[9] with on-site nonmagnetic disorders. In tight-binding representation on a square lattice, it gives[4]

$$H = \sum_{\mathbf{i}} \epsilon_{\mathbf{i}} \psi_{\mathbf{i}}^{\dagger} \psi_{\mathbf{i}} + (t_x \psi_{\mathbf{i}}^{\dagger} \psi_{\mathbf{i}+\hat{x}} + t_y \psi_{\mathbf{i}}^{\dagger} \psi_{\mathbf{i}+\hat{y}} + h.c.), \quad (1)$$

where $\psi_{\mathbf{i}} = (\psi_{\mathbf{i}s\uparrow}, \psi_{\mathbf{i}p\uparrow}, \psi_{\mathbf{i}s\downarrow}, \psi_{\mathbf{i}p\downarrow})^{\mathrm{T}}$ is the field for the four orbital states, $|s,\uparrow\rangle, |p_x+ip_y,\uparrow\rangle, |s,\downarrow\rangle, |-p_x+ip_y,\downarrow\rangle$, on site $\mathbf{i} = (m,n)$, and $\epsilon_{\mathbf{i}}$ and $t_{x(y)}$ are respectively the on-site energy as well as the overlap integral matrices along $x(y)$ direction, which are explicitly

$$\epsilon_{\mathbf{i}} = \mathrm{Diag}(\epsilon_{\mathrm{s}} + \Delta_{\mathbf{i}}, \epsilon_{\mathrm{p}} + \Delta_{\mathbf{i}}, \epsilon_{\mathrm{s}} + \Delta_{\mathbf{i}}, \epsilon_{\mathrm{p}} + \Delta_{\mathbf{i}}), \quad (2)$$

$$t_x = \begin{pmatrix} \frac{D+B}{a^2} & \frac{-iA}{2a} & 0 & 0 \\ \frac{-iA}{2a} & \frac{D-B}{a^2} & 0 & 0 \\ 0 & 0 & \frac{D+B}{a^2} & \frac{iA}{2a} \\ 0 & 0 & \frac{iA}{2a} & \frac{D-B}{a^2} \end{pmatrix}, \quad (3)$$

$$t_y = \begin{pmatrix} \frac{D+B}{a^2} & \frac{A}{2a} & 0 & 0 \\ \frac{-A}{2a} & \frac{D-B}{a^2} & 0 & 0 \\ 0 & 0 & \frac{D+B}{a^2} & \frac{A}{2a} \\ 0 & 0 & \frac{-A}{2a} & \frac{D-B}{a^2} \end{pmatrix}. \quad (4)$$

In the above, a is the lattice constant, A,B,C,D,M are material parameters depending on the QW width[9], $\epsilon_{s(p)} = C \pm M - 4(D \pm B)/a^2$, and $\Delta_{\mathbf{i}}$ is the on-site disorder energy for nonmagnetic impurities, which is identical for the four orbitals and uniformly distributed in $[-W/2, W/2]$ with disorder strength W. To compare

with the previous works, we use the same values for the parameters as in Refs.[2,4], i.e., $A = 364.5$ meV·nm, $B = -686$ meV·nm^2, $C = 0$, $D = -512$ meV·nm^2, $M = 1$ meV and $a = 5$ nm.

The method of twisted boundary conditions[13,14] is used in this work to directly diagonalize the disordered system, and the transfer matrix method[11] is taken to obtain the wave-function distributions.

Without disorder, the mass parameter M characterizes the effect of band inversion by changing its sign from positive to negative, and results in a topological phase transition from a conventional insulating state ($M > 0$) to a quantum spin Hall phase ($M < 0$) with a single pair of helical edge states at each boundary. This pair of helical edge states is clearly seen in energy-momentum space by diagonalizing the clean Hamiltonian (setting $\Delta_{\mathbf{i}} = 0$ in Eq.(1)). However, for disordered systems, the translational symmetry is generally broken and the momentum is not a good quantum number anymore. But if we view the disordered system of size $L_x \times L_y$ as a cell of an infinite one, and fold it into a cylinder with longitudinal axis in y-direction, then the translational symmetry is restored, where a particle gains an extra phase factor $e^{i\phi_x}$ whenever it goes across the boundary in the x-direction. In such a case, $-\pi \leq \phi_x \leq \pi$, plays the role of the generalized momentum, and we could diagonalize the disordered system in $E - \phi_x$ plane and study the edge properties as a function of W. It should be noted that the choice of L_x should be larger than the average decay length of the wave-functions. It is found that $L_x = 15a$ is good enough for diagonalization, and we set $L_y = 100a$ all throughout the paper unless mentioned in particular.

Wave-functions study takes its special advantages to gain insights of how a conventional insulating state transits into a topological nontrivial phase and vice versa. To obtain the wave-functions in real space, we consider a two-terminal setup as seen in Fig.1, and adopt the standard transfer matrix method[11] with the iteration equation along x direction written as

$$\begin{pmatrix} \Psi(m+1) \\ \Psi(m) \end{pmatrix} = M(m) \begin{pmatrix} \Psi(m) \\ \Psi(m-1) \end{pmatrix}, \quad (5)$$

where $\Psi(m) = (\psi_{m1}, \psi_{m2}, \cdots, \psi_{mL_y})^{\mathrm{T}}$ is the wave-function vector at slice $x = m$, and $M(m)$ is the corresponding transfer matrix. In the region of disordered HgTe/CdTe QWs, the transfer matrix reads explicitly

$$M(m) = \begin{pmatrix} T_x^{-1}[E_f I - H(m)] & -T_x^{-1}T_x^{\dagger} \\ I & O \end{pmatrix}, \quad (6)$$

where E_f is the Fermi energy of the clean system, I and O are respectively the $4L_y \times 4L_y$ unit and null matrices, and

$$T_x = \mathrm{Diag}(t_{\mathrm{x}}, t_{\mathrm{x}}, \cdots, t_{\mathrm{x}}) \quad (7)$$

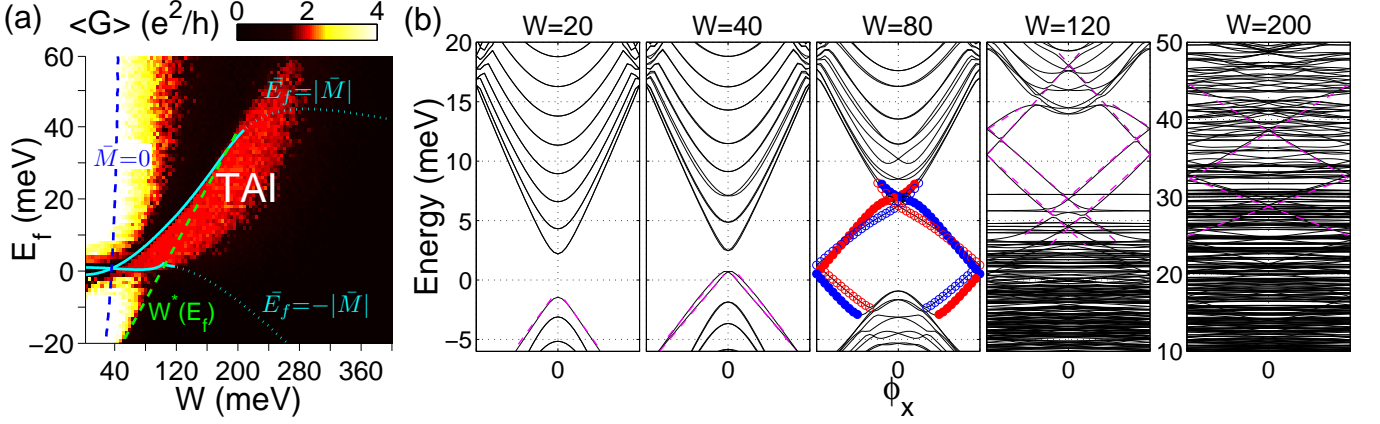is the block diagonal overlap matrix with the same di-

FIG. 2: (color online). (a) Phase diagram of disordered HgTe/CdTe QWs on $E_f - W$ plane, which is simulated from a stripe geometry with $L_x = 500a$ and $L_y = 100a$. The curves are theoretical results obtained from the SCBA. The blue dashed line represents the interface $\bar{M} = 0$, to the right of which the mass parameter is renormalized to negative. The green dashed line is the border where the self-energy becomes imaginary. The TAI phase is indicated as the crescent-shaped region where the phase boundaries, $|\bar{E}_f| = \pm|\bar{M}|$, are marked by the solid cyan lines. It is seen that the SCBA fails at strong-disorder boundary as denoted by the dotted parts. (b) The evolutions of TAI's energy spectrum with disorder strength W in the generalized momentum space. In the subfigure of $W = 80$, the edge states are labeled according to their density distributions (empty and solid circles) as well as the spin polarization (blue and red). The purple dashed lines in the other subfigures are guides for the eyes of the edge states dispersions.

mension, while

$$
H(m) = \begin{pmatrix} \epsilon(m,1) & t_y & & & \\ t_y^{\dagger} & \epsilon(m,2) & t_y & & \\ & . & . & . & \\ & & t_y^{\dagger} & \epsilon(m,n) & t_y \\ & & & . & . & . \end{pmatrix} \quad (8)
$$

is the block-tridiagonal slice Hamiltonian with open boundary conditions in y-direction. By applying a small external bias, we can calculate the longitudinal conductance using the Landauer-Büttiker formulae[11,15] as well as the wave-functions on each site. Fig.2(a) shows the TAI phase diagram reproduced by the transfer matrix method, which is in good consistent with the previous works[2,5].

In the following, we first explore the evolution of the energy spectrum in the generalized momentum space with disorder strength W, and then study the topological phase transition in the viewpoint of real space wavefunctions. The obtained results agree with each other well, which also validates our numerical methods.

III. NUMERICAL RESULTS

A. Overview of the phase diagram

Let us first review the numerical and theoretical results of the TAI phase diagram[2,5], which is reproduced in Fig.2(a) with the stripe length $L_x = 500a$.

Numerically the TAI phase is identified by the suddenly appeared quantized conductance, $2e^2/h$, as the in-

creasing of W at fixed E_f. See the crescent-shaped region in Fig.2(a), where the statistical fluctuations are vanishing small. This region has a clear-cut weak-disorder boundary at which the TAI phase begins but a blurred strong-disorder boundary where the TAI phase terminates.

Theoretically the transitions into the TAI phase at the weak-disorder boundary can be understood within the the SCBA[3,5]. It is demonstrated that the random potential renormalizes both the Fermi energy and the mass parameter as a function of disorder strength, $\bar{E}_f(W)$ and $\bar{M}(W)$, so that starting from a metallic phase, the mass changes sign when across some critical disorder strength, and the TAI phase is defined by the combination of conditions $\bar{M} < 0$ as well as $-|\bar{M}| < \bar{E}_f < |\bar{M}|$. In Fig.2(a), the boundary $\bar{M}(W) = 0$, which separates the positive and negative effective mass is plotted as blue dashed line, and the band edges, $\bar{E}_f = \pm\bar{M}$, obtained from the SCBA are shown in cyan. It is seen that the results predicted from the SCBA agree very well with the weak-disorder boundary of the TAI phase obtained from our numerical simulations. However the SCBA fails to give the correct strong-disorder boundaries, as seen by the dotted parts of the cyan lines.

Physically the strong-disorder boundary is blurred because in this region there are impurity states enter into the renormalized bulk gap, which embodies in the property that the self-energy has a nonvanishing imaginary part[3]. In Fig.2(a), the critical disorder strength is shown as a function of Fermi energy, $W^*(E_f)$, see the green dashed line, where for $W > W^*$ the self-energy becomes imaginary. This line distinguishes the TAI phase into two
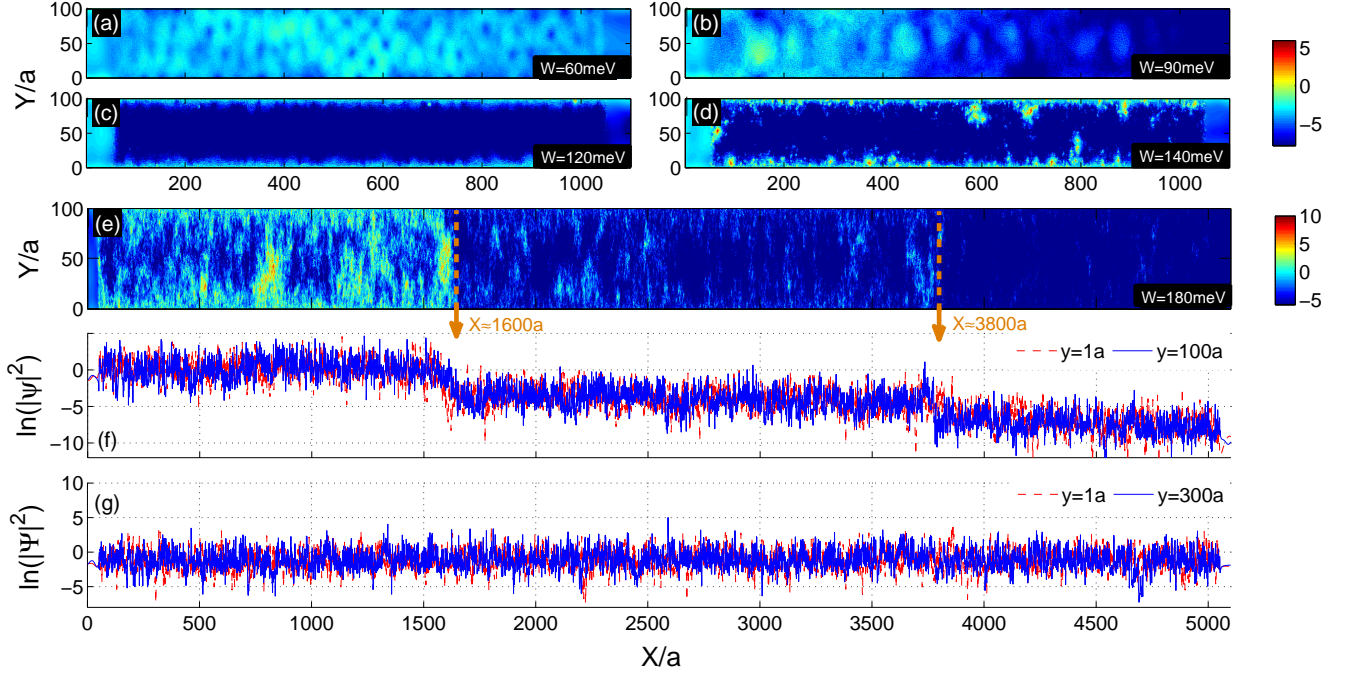
FIG. 3: (Color online). Logarithmic wave-function intensities at $E_f = 10$ meV. The wave-function intensities before, on, and at the tail of the TAI plateau are shown respectively in (a)-(b), (c)-(d), and (e). The edge states wave-function intensities in (e) at $y = 1a$ and $100a$ are given in (f), where the brown arrows indicate the positions where accidental couplings between the edge states occur due to the large fluctuations of the local decay length. For comparison, the edge states wave-function intensities of a wider stripe with $L_y = 300a$ are plotted in (g) with all the other parameters remain the same as in (e). In all the figures, the first and last 50 lattices are leads region.

regions by whether the band edges are effectively defined or not. If they are not, the mobility edges should play the role.

Finally we note that the strong-disorder boundary is expected to be an Anderson transition boundary[3,5,7], however a direct scaling analysis of Anderson transitions is still absent, which we will present below.

B. Evolutions of edge states with disorder strength

As mentioned above, the observed quantized conductance plateau in TAI phase is attributed to the presence of conducting edge states induced by disorder. However, the existence of such edge states has never been shown directly in the TAI's energy spectrum. In this section, we first diagonalize the HgTe/CdTe QWs for a specific disorder realization with increasing disorder strength W (meV). The twisted and open boundary conditions are used respectively in x and y directions. The obtained energy spectrum is in $E - \phi_x$ plane, and five representatives with $W = 0$, 40, 80, 120 and 200 are given in Fig.2(b)[16].

In the clean limit where $W = 0$, we see that the spectrum exhibits a topological-trivial feature with a full bulk gap $E_g \simeq 2|M|$ (the derivations are due to the finite size of L_y), which inversely proves the validity of our method. With the increasing of the disorder strength,

say to $W = 40$, it is seen that though the system still behaves like a normal insulator, there are trivial edge states (see the dashed purple lines) grown up from the lower band and the bulk gap becomes much narrower. In fact, we have observed the closing of band gap around $W_c = 50$ (for our particular disorder realization) and its reopening immediately at a bit larger disorder strength, but with the presence of two pairs of gapless edge states. Since the phase transition necessarily accompanies with gap-closing[17], we speculate that the system transits into the TAI phase for $W > W_c$, and a typical spectrum after this transition is exemplified at $W = 80$. The observation of the gapless edge states with nonvanishing disorders in generalized momentum space provides the most direct evidence so far that it is the disorder-induced edge transport which leads to the quantized conductance in TAI phase. Moreover, these gapless edge states persist to even stronger disorder strength, nevertheless the low energy states begin to localize and smear the band edges, see the $W = 120$ figure for example, which is in good consistent with the phase diagram. Interesting thing happens in the strong-disorder region. With strong-disorder, naively we would expect that all states are localized and the system becomes an Anderson insulator. However, the energy spectrum at $W = 200$ shows that although the bulk gap is completely smeared by the impurity states and the band edges are ill-defined, the edge states are

still robust and winding around the projected Brillouin zone.

To compare with the helical properties[18] of the edge states in clean HgTe/CdTe QWs, we have studied the edge states with disorder in detail by analyzing their eigen-functions. The results are shown in the sub-figure with $W = 80$. The edge states are labeled according to their density distributions $\rho(y) = \int dx \Psi^\dagger(\vec{i})\Psi(\vec{i})$ as well as the spin polarization $\vec{s}(y) = \int dx \Psi^\dagger(\vec{i})\vec{\sigma}\Psi(\vec{i})$, where the solid (empty) circles indicate the states exponentially localized near the $y = 0$ (L_y) boundary, and the color red (blue) represents the up (down) spin polarization. The helical character of these edge states for a given energy is clearly seen, where there is a single Kramer's pair at each edge with spin-momentum locking. The whole spectrum preserves the time-reversal symmetry by observing that $E_{n\alpha}(\phi_x) = E_{n\bar{\alpha}}(-\phi_x)$, where n is the band index and $\alpha = \uparrow, \downarrow$, which is a result of nonmagnetic disorders. Whereas the spin degeneracy is lifted due to the breaking of inversion symmetry by disorder. At the time-reversal invariant points, $\phi_x = 0, \pi$, the edge states switch their Kramer's partners[19], which leads to a nontrivial topology. This is also confirmed by calculating the Z_2 index ν_0 of this 2D system with the twisted boundary conditions on both directions following the method in Ref.[7]. All these results strongly support the statement that the transition from a normal insulator at $W = 0$ to TAI is a topological one, and the quantized conductance plateau originates from the disorder-induced conducting helical edge states which are intrinsic to TAI.

C. Edge states destruction at strong disorder

The robustness of the disorder-induced edge states shown in Fig.2(b) (the sub-figure with $W = 200$) naturally raises the questions that how will these edge states be destroyed in strong-disorder region, and what is their difference with the exponential localization of bulk states? Not like the case where the edge states themselves could be localized by magnetic perturbations, with non-magnetic disorders, the edge states decay only through the coupling with each other. For a finite-width system, this generally depends on the competition between the localization length $\xi(W)$ of bulk states and the system width L_y. Only if $\xi(W) \sim L_y$, even localized bulk states can couple the edge states at opposite boundaries and destroy the edge states, thus we may expect something interesting to happen. While for an infinite system, only extended states can couple the edge states far away from each other, therefore a localization-delocalization Anderson transition is expected, which is the true strong-disorder boundary of TAI phase. In this section, we investigate the decay mechanism of the disorder-induced edge states for a finite-width system by studying its wave-functions in real space. The scaling analysis of Anderson transitions for an infinite system is discussed in the next section.
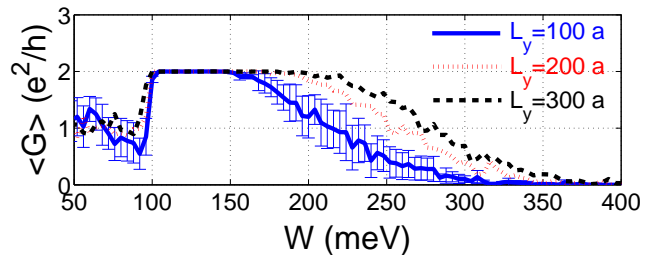

FIG. 4: (color online). The average conductance $\langle G \rangle$ versus disorder strength W for different system width at $E_f = 10$ meV. Each line is averaged from 100 disorder realizations and $L_x = 500a$. The fluctuations are only shown for the line of $L_y = 100a$.

We first let $L_x = 10^3 a$ and fix $E_f = 10$ meV. The logarithmic wave-function distributions before, on, and at the tail of conductance plateau are given respectively in Figs.3(a)-(b), (c)-(d), and (e). Before the TAI plateau, we see that the bulk states are weakened with the enhancement of disorder strength. When on the TAI plateau, the bulk states disappear completely and two propagating 1D edge states are seen clearly, which contribute a quantized conductance e^2/h per edge. However, with the increase of disorder strength, the bulk states reappear and begin to localize but coexist with the conducting edge states, as seen in Fig.3(d). This is equivalent to the $W = 120$ case in Fig.2(b) in the generalized momentum space where the band edges are ill-defined but the mobility edge starts to count. We see that the wave-function behaviors in real space agree very well with the pictures presented above when studying the energy spectrum.

Interesting thing happens when we move to the tail of TAI plateau, as seen in Fig.3(e) where a longer length $L_x = 5 \times 10^3 a$ is set. With periodic boundary conditions on both directions, only bulk states exist, which decay exponentially in the propagating direction[11]. Differently here, with open boundary conditions in one direction, we see that the edge states fade in three segments as indicated by the brown arrows, and decay much slower with localized bulk states in between. To check the interplay between these localized bulk states and the edge states, we choose two lines at $n = 1$ and 100 and plot the logarithmic intensities of their wave-functions in Fig.3(f). It is striking to find that the edge states decay in a *stepwise* pattern in contrast to the exponential way. This unusual behavior can be understood by the *accidental coupling* between the edge states at opposite boundaries assisted by the localized bulk states due to the fluctuations of the decay length L_d. It is estimated that $\xi \simeq \langle L_d \rangle \sim 10a$ at this disorder strength, which is comparable to L_y, and the intensities of edge states wave-functions drop off approximately at the interfaces of each segment, $m = 1600$ and 3800, where the local decay length, $L_d(m)$, is large. To check this, we enlarge the system width to $L_y = 300a$,
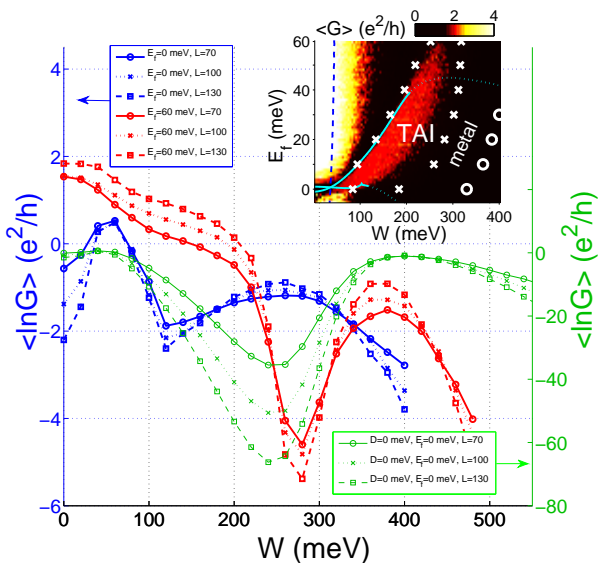
FIG. 5: (color online). Scaling behavior of average logarithmic conductance as a function of W at differnet energies $E_f = 60$ and 0 meV. The red and blue curves are calculated with nonvanishing quadratic kinetic term while the green curves are calculated by setting $D = 0$. The blue and red curves are scaled by the left axis, and the green curves are scaled by the right axis. Inset: the Anderson transitions obtained from the scaling analysis are marked by white symbols in the phase diagram.

and the corresponding edge states wave-function intensities at $n = 1$ and 300 are given in Fig.3(g). In this case, we have $\xi \simeq \langle L_d \rangle \ll L_y$, therefore a longer system length is needed for the accidental coupling between the edge states to happen. For the current simulation, it is seen that the edge states persist throughout the system, and no coupling occurs at the much larger scale of $5 \times 10^3 a$.

D. Scaling analysis of Anderson transitions

The above wave-function analysis shown in Figs.3(f)-(g) implies that the range of the TAI plateau is system-size dependent. For a fixed length L_x, the wider the width of the system is, the broader the conductance plateau will be. This is indeed true as seen in Fig.4 where the conductance plateaus for $L_y = 100a$, $200a$ and $300a$ at $L_x = 500a$ are presented. What will happen as L_y tends to infinite? For an infinite system, if the bulk states keep localized, where the localization length ξ has a finite value, then the edge transports, so that the conductance plateaus, will not be destroyed no matter how large the ξ is. Thus the TAI phase disappears in an infinite system only when the bulk states become delocalized and ξ is divergent. Therefore a localization-delocalization Anderson transition is expected, which kills the TAI phase in strong-disorder region.

To see the existence of such an Anderson transition,

we carry out the scaling analysis of the bulk conductance using periodic boundary conditions[11]. The average logarithmic conductance, $\langle LnG \rangle$, on $E_f - W$ plane is calculated for different system sizes $L_x = L_y = L$, and the average is performed under 2×10^3 disorder realizations. For each E_f, the Anderson transitions are recognized as the crossings of the $\langle LnG(W) \rangle$ lines with different L's, as seen in Fig.5. And in each region between two crossings, the system is judged to be in insulating (metallic) if $\langle LnG \rangle$ increases as the decrease (increase) of L at a fixed W. For example, there are three Anderson transitions at $E_f = 60$ meV as indicated by the red lines in Fig.5, where the system first transits from metallic to insulating, which corresponds to the weak-disorder boundary of the TAI phase obtained by SCBA; then transits from this topological insulating phase to metallic again, which is the localization-delocalization strong-disorder boundary of the TAI phase we expect. After the third transition, the whole system is totally localized and becomes an Anderson insulator. The complete result is given in the inset of Fig.5, where the Anderson transitions are marked as white symbols on the phase diagram. The region enclosed by the white crosses is the TAI island, and we see that this region is much wider than the simulation result for a finite-width system.

The conductance scaling at $E_f = 0$ is also shown as blue lines in Fig.5. It is interesting to compare our results with the recent work of Ref.[12], where only a special energy point $E_f = 0$ is considered, and the kinetic term, Dk^2, is omitted. It is concluded there that in the presence of an extra spin s_z-conservation breaking term, the Rashba spin-orbit coupling, in the HgTe/CdTe QWs, a finite metallic region is found which partitions the two topological distinct insulating phases. However, our results demonstrate that the metallic region which separates the TAI and the Anderson insulator phases can exist by inclusion the quadratic kinetic term or tuning the E_f to higher energies even with the spin s_z-conservation, and the Rashba term is not necessary. This is the direct result of the localization-delocalization Anderson transition we predict. In Fig.5, the scaling behavior of conductance at $E_f = 0$ by setting the parameter $D = 0$ is shown as green lines, where we see that the metallic region in-between the TAI and the Anderson insulator phases disappear indeed, which is the case discussed in Ref.[12].

IV. CONCLUSIONS

In summary, the system of disordered HgTe/CdTe QWs is studied. The evolution of its energy spectrum in the generalized momentum space with the disorder strength is obtained, where the existence of topologically protected helical edge states in the TAI phase is demonstrated directly, which proves the conjecture that they are responsible for the observed quantized conductance plateau. With nonmagnetic perturbations which

preserve the time-reversal symmetry of the system, the edge states can be destroyed only through the coupling with each other. For a finite-width system, it is shown that the edge states decay in a *stepwise* pattern assisted with the localized bulk states due to the fluctuations of the decay length, which is in extraordinarily contrast with the exponential decay of bulk states. While for an infinite system, the edge states can become decoherent only through the coupling with extended states, therefore a localization-delocalization Anderson transition is expected in strong-disorder region, which is confirmed by the scaling analysis. Moreover, multiple Anderson transitions are also obtained, where in particular, a metallic region which separates two topologically distinct insulating phases is found by inclusion of the quadratic kinetic term or turning E_f to higher energies without an extra spin s_z-nonconservation term. These results are also expected to be valid for 3D TAI[3].

[1] For reviews, see J. E. Moore, Nature (London) **464**, 194 (2010); M. Z. Hasan and C. L. Kane, Rev. Mod. Phys. **82**, 3045 (2010); X. L. Qi, S. C. Zhang, arXiv:1008.2026v1.

[2] J. Li, R. L. Chu, J. K. Jain, S. Q. Shen, Phys. Rev. Lett. **102**, 136806 (2009).

[3] H. M. Guo, G. Rosenberg, G. Refael, and M. Franz, Phys. Rev. Lett. **105**, 216601 (2010).

[4] H. Jiang, L. Wang, Q. F. Sun, X. C. Xie, Phys. Rev. B **80**, 165316 (2009).

[5] C. W. Groth, M. Wimmer, A. R. Akhmerov, J. Tworzydlo, C. W. J. Beenakker, Phys. Rev. Lett. **103**, 196805 (2009).

[6] E. Prodan, Phys. Rev. B **83**, 195119 (2011).

[7] H. M. Guo, Phys. Rev. B **82**, 115122 (2010).

[8] E. Prodan, J. Phys. A: Math. Theor. **44** 113001 (2011).

[9] B. A. Bernevig, T. L. Hughes, S.-C. Zhang, Science **314**, 1757 (2006).

[10] M. König, S. Wiedmann, C. Brne, A. Roth, H. Buhmann, L. W. Molenkamp, X.-L. Qi, S.-C. Zhang, Science **318**, 766 (2007).

[11] A. MacKinnon, B. Kramer, Phys. Rev. Lett. **47**, 1546 (1981); Z. Physics. B **53**, 1 (1983).

[12] A. Yamakage, K. Nomura, K. Imura, Y. Kuramoto, J. Phys. Soc. Jpn. **80**, 053703 (2011).

[13] Q. Niu, D.J. Thouless, and Y.-S. Wu, Phys. Rev. B **31**, 3372 (1985).

[14] X.-L. Qi, Y.-S. Wu, and S.-C. Zhang, Phys. Rev. B **74**, 045125 (2006).

[15] R. Landauer Philos. Mag. 21, 863 (1970).

[16] See Fig.1 in the supplemental material where a complete evolution of the energy spectrum is given.

[17] S. Murakami, S. Iso, Y. Avishai, M. Onoda, N. Nagaosa, Phys. Rev. B **76**, 205304 (2007).

[18] C. Wu, B. A. Bernevig, and S.-C. Zhang, Phys. Rev. Lett. **96**, 106401 (2006).

[19] L. Fu, C. Kane, Phys. Rev. B **74**, 195312 (2006).